

Spectroscopic and Electrochemical Properties of (μ -Oxo)diiron(III) Complexes Related to Diiron-Oxo Proteins. Structure of $[\text{Fe}_2\text{O}(\text{TPA})_2(\text{MoO}_4)](\text{ClO}_4)_2$

Richard C. Holz,[†] Timothy E. Elgren,[†] Linda L. Pearce,[†] Jian H. Zhang,[‡] Charles J. O'Connor,[‡] and Lawrence Que, Jr.,^{*†}

Departments of Chemistry, University of Minnesota, Minneapolis, Minnesota 55455, and University of New Orleans, New Orleans, Louisiana 70122

Received March 3, 1993[®]

A series of (μ -oxo)diiron(III) complexes of tris(2-pyridylmethyl)amine (TPA), $[\text{Fe}_2\text{O}(\text{TPA})_2(\text{L})](\text{ClO}_4)_2$, were synthesized and characterized where L represents the bridging tetraoxo anion ligands sulfate, phosphate, arsenate, vanadate, and molybdate. These tetraoxo anion complexes are the first (μ -oxo)diiron(III) complexes that reproduce the protein-tetraoxo anion stoichiometry found in purple acid phosphatases (PAPs). $[\text{Fe}_2\text{O}(\text{TPA})_2(\text{MoO}_4)](\text{ClO}_4)_2$ (**9**) crystallizes in the monoclinic space group $P2_1/n$ ($a = 12.74(1)$ Å, $b = 24.69(2)$ Å, $c = 13.733(8)$ Å, $\beta = 103.41(7)^\circ$, and $Z = 4$) and consists of two distinct six-coordinate Fe(III) centers bridged by oxo and molybdate. **9** represents the first (μ -oxo)diiron(III) complex with a single bridging molybdate to be structurally characterized. These new complexes together with previously reported (μ -oxo)diiron(III) TPA complexes constitute a series with a wide range of Fe- μ -O-Fe angles and bridging anion basicities which affect their electronic absorption, resonance Raman, and electrochemical properties. A linear correlation between the Raman $\nu_6(\text{Fe}-\text{O}-\text{Fe})$ mode and the energy of the long-wavelength visible absorption band provides a method in which UV-vis spectroscopy can be used to estimate the Fe-O-Fe angle. The electrochemical properties of these complexes show the expected dependence on charge and basicity and thus serve as a basis on which to interpret the redox properties of diiron-oxo proteins, particularly uteroferrin, the purple acid phosphatase from porcine uterus. Comparison of the electrochemical properties of the phosphate, arsenate, and molybdate complexes in the (μ -oxo)diiron(III) TPA series with those of corresponding complexes of uteroferrin suggests that both phosphate and arsenate bridge the diiron core in uteroferrin, while molybdate must bind only to the redox inactive Fe(III) center. The mixed-valent forms of several of these complexes exhibit EPR signals with $g_{av} < 2$, like those observed for the mixed-valent diiron enzymes but with smaller g anisotropies.

Introduction

The structural, electronic, and vibrational properties of (μ -oxo)diiron(III) centers have been the subject of intense study in recent years because of their presence in non-heme iron proteins.^{1,2} Enzymes in this class include hemerythrin (Hr), the R2 protein of ribonucleotide reductase (R2), the hydroxylase component of methane monooxygenase (MMO), and the purple acid phosphatases (PAPs) from porcine uteri (uteroferrin (Uf)) and bovine spleen (BSPAP).² Both Hr and R2, in their diferric forms, have been characterized extensively by various spectroscopic methods as well as X-ray crystallography.^{2a,c,3,4} MetHr contains a (μ -oxo)bis(μ -carboxylato)diiron(III) core, while metR2 contains a (μ -oxo)(μ -carboxylato)diiron(III) core. Several (μ -oxo)diiron(III) complexes with one or two bridging carboxylate groups have been synthesized.^{1b,2a,5,6} These complexes model the active

sites of metHr and metR2; however, only a few complexes which serve as models for the diiron active site of PAPs have been reported.^{6,7}

PAPs are known to interact with tetraoxo anions such as phosphate, arsenate, vanadate, and molybdate, all of which inhibit phosphatase activity.^{2b} Phosphate and arsenate are weak inhibitors and potentiate the aerobic oxidation of the reduced enzyme while molybdate is a strong inhibitor and stabilizes the reduced form. Furthermore, these inhibitors alter the spectroscopic and physical properties of the diiron core; however, their specific mode of binding to the diiron active site remains unclear. While possible structures have been proposed,^{8,9} suitable models for many of these interactions are lacking. A few dinuclear complexes which serve as models for phosphate and arsenate binding have been reported.⁷ Even though these studies were rich in structural detail, none of them represented a systematic investigation of the effects of each of these anions on a dinuclear iron core.

We recently reported the syntheses, structures, and spectral properties of several (μ -oxo)diiron(III) complexes of tris(2-pyridylmethyl)amine (TPA) in which the Fe-O-Fe angle was systematically increased.¹⁰ The use of the tetradentate tripodal

[†] University of Minnesota.

[‡] University of New Orleans.

[®] Abstract published in *Advance ACS Abstracts*, November 15, 1993.

- (1) (a) Murray, K. S. *Coord. Chem. Rev.* **1974**, *12*, 1-35. (b) Kurtz, D. M., Jr. *Chem. Rev.* **1990**, *90*, 585-606.
- (2) (a) Que, L., Jr.; True, A. E. *Prog. Inorg. Chem.* **1990**, *38*, 97-200. (b) Vincent, J. B.; Averill, B. A. *FASEB J.* **1990**, *4*, 3009-3014. (c) Sanders-Loehr, J. In *Iron Carriers and Iron Proteins*; Loehr, T. M., Ed.; VCH Publishers: New York, 1989; pp 373-466. (d) Wilkins, P. C.; Wilkins, R. G. *Coord. Chem. Rev.* **1987**, *79*, 195-214.
- (3) (a) Stenkamp, R. E.; Sieker, L. C.; Jensen, L. H. *J. Am. Chem. Soc.* **1984**, *106*, 618-622. (b) Sheriff, S.; Hendrickson, W. A.; Smith, J. L. *J. Mol. Biol.* **1987**, *197*, 273-296. (c) Holmes, M. A.; Trong, I. L.; Turley, S.; Sieker, L. C.; Stenkamp, R. E. *J. Mol. Biol.* **1991**, *218*, 583-593.
- (4) Nordlund, P.; Sjöberg, B.-M.; Eklund, H. *Nature* **1990**, *345*, 593-598.
- (5) (a) Armstrong, W. H.; Spool, A.; Papaefthymiou, G. C.; Frankel, R. B.; Lippard, S. J. *J. Am. Chem. Soc.* **1984**, *106*, 3653-3667. (b) Hartman, J. R.; Rardin, R. L.; Chaudhuri, P.; Pohl, K.; Wieghardt, K.; Nuber, B.; Weiss, J.; Papaefthymiou, G. C.; Frankel, R. B.; Lippard, S. J. *J. Am. Chem. Soc.* **1987**, *109*, 7387-7396.

- (6) (a) Yan, S.; Cox, D. D.; Pearce, L. L.; Juarez-Garcia, C.; Que, L., Jr.; Zhang, J. H.; O'Connor, C. J. *Inorg. Chem.* **1989**, *28*, 2507-2509. (b) Norman, R. E.; Yan, S.; Que, L., Jr.; Backes, G.; Ling, J.; Sanders-Loehr, J.; Zhang, J. H.; O'Connor, C. J. *J. Am. Chem. Soc.* **1990**, *112*, 1554-1562.
- (7) (a) Armstrong, W. H.; Lippard, S. J. *J. Am. Chem. Soc.* **1985**, *107*, 3730-3731. (b) Turowski, P. N.; Armstrong, W. H.; Roth, M. E.; Lippard, S. J. *J. Am. Chem. Soc.* **1990**, *112*, 681-690. (c) Drücke, S.; Wieghardt, K.; Nuber, B.; Weiss, J.; Fleischhauer, H.-P.; Gehring, S.; Haase, W. *J. Am. Chem. Soc.* **1989**, *111*, 8622-8631. (d) Drücke, S.; Wieghardt, K.; Nuber, B.; Weiss, J. *Inorg. Chem.* **1989**, *28*, 1414-1417.
- (8) David, S. S.; Que, L., Jr. *J. Am. Chem. Soc.* **1990**, *112*, 6455-6433.
- (9) Vincent, J. B.; Crowder, M. W.; Averill, B. A. *Biochemistry* **1992**, *31*, 3033-3037.

ligand TPA allows only one bridging ligand to bind; thus a series of (μ-oxo)diiron(III) complexes with a bridging tetraoxo anion such as sulfate, phosphate, arsenate, vanadate, and molybdate could be synthesized. These tetraoxo anion complexes are the only ones that reproduce the protein-anion stoichiometry found in PAPs. With this enlarged series of (μ-oxo)diiron(III) TPA complexes, we have systematically investigated the angular dependence of the electronic spectral properties of the Fe–O–Fe unit, its electrochemical properties as a function of bridging ligand, and the EPR properties of the mixed-valent forms.

Experimental Methods

Synthetic Methods. TPA·3HClO₄ was synthesized according to literature procedures,¹¹ while all other chemicals were purchased commercially and used as received. *Caution!* The perchlorate salts in this study are all potentially explosive and should be handled with care.

The various [Fe₂O(TPA)₂(L)](ClO₄)_x complexes were all synthesized in a similar manner. A typical preparation is as follows:¹⁰ TPA·3HClO₄ (0.59 g, 1.0 mmol) and triethylamine (0.56 mL, 4.0 mmol) in 40 mL of MeOH were reacted with Fe(ClO₄)₃·xH₂O (0.54 g, 1.0 mmol) dissolved in 2 mL of MeOH. To this mixture was added a solution of the bridging ligand (0.5 mmol) and triethylamine (0.5 or 1.0 mmol, depending on the number of protons to be neutralized) in H₂O (≈2 mL). A solid was obtained from the reaction mixture and crystallized by vapor diffusion of diethyl acetate into a filtered acetonitrile solution of the complex. The analytical purity of each complex was checked by elemental analysis (Desert Analytics). Anal. Calcd for [Fe₂O(TPA)₂(SO₄)](ClO₄)₂·2H₂O·CH₃CN (4) (C₃₈H₄₃N₉O₁₅Cl₂Fe₂S): C, 42.24; H, 4.01; N, 11.67. Found: C, 41.60; H, 3.76; N, 11.60. Calcd for [Fe₂O(TPA)₂(HPO₄)](ClO₄)₂ (5) (C₃₆H₃₇N₈O₁₃Cl₂Fe₂P): C, 43.10; H, 3.72; N, 11.17. Found: C, 42.74; H, 3.53; N, 10.95. Calcd for [Fe₂O(TPA)₂(HASO₄)](ClO₄)₂ (7) (C₃₆H₃₇N₈O₁₃Cl₂Fe₂As): C, 41.29; H, 3.56; N, 10.70. Found: C, 41.51; H, 3.78; N, 10.59. [Fe₂O(TPA)₂(HVO₄)](ClO₄)₂·H₂O (8) (C₃₆H₃₉N₈O₁₄Cl₂Fe₂V): C, 41.53; H, 3.78; N, 10.76. Found: C, 41.67; H, 3.77; N, 10.66. [Fe₂O(TPA)₂(MoO₄)](ClO₄)₂·CH₃CN·H₂O (9) (C₃₈H₃₉N₉O₁₃Cl₂Fe₂Mo): C, 40.52; H, 3.67; N, 11.19. Found: C, 40.53; H, 3.93; N, 10.97. The newly synthesized complexes were also characterized by their characteristic NMR spectra (Table SI) and UV–vis spectra (Table IV). All of these data are consistent with those previously reported for [Fe₂O(TPA)₂(L)](ClO₄)_{2 or 3} complexes.^{6b,10}

Crystallographic Studies. Olive platelike crystals of [Fe₂O(TPA)₂(MoO₄)](ClO₄)₂·CH₃CN (9), suitable for X-ray diffraction studies, were grown from acetonitrile/ethyl acetate. An appropriate crystal having approximate dimensions of 0.35 × 0.25 × 0.02 mm was mounted on a glass fiber coated with a viscous high-molecular-weight hydrocarbon. All data were collected at the Crystallographic Facility of the University of Minnesota Chemistry Department on an Enraf-Nonius CAD4 diffractometer using graphite-monochromated Mo Kα (λ = 0.710 69 Å) radiation by the ω-scan method at –88 °C. All data were corrected for Lorentz and polarization effects. Three standard reflections were measured every 75 min and remained constant throughout data collection. The structure was solved using direct methods, and empirical absorption corrections were made using the program DIFABS,¹² resulting in transmission factors ranging from 0.83 to 1.22. All non-hydrogen atoms except those of the acetonitrile solvate were refined anisotropically.¹³ Refinement was carried out on *F* using a full-matrix least-squares procedure, with scattering factors from ref 14 which include anomalous dispersion terms.¹⁵ Hydrogen atoms were placed in their calculated positions, assigned thermal parameters which were 20% greater than the *B*_{eq} value of the atom to which they were bonded, and included in the structure factor calculations. Pertinent crystallographic details for 9 are collected in Table I, atomic coordinates for the non-hydrogen atoms are listed in Table II, and selected bond lengths and angles are tabulated in Table III. The complete listings

Table I. Crystal Structure Parameters of [Fe₂O(TPA)₂(MoO₄)](ClO₄)₂·CH₃CN

empirical formula	C ₃₈ H ₃₉ Cl ₂ Fe ₂ N ₉ O ₁₃ Mo
fw	1108.33
<i>T</i> (°C)	–88
crystal system	monoclinic
space group	<i>P</i> 2 ₁ / <i>n</i> (No. 14)
<i>a</i> (Å)	12.74(1)
<i>b</i> (Å)	24.69(2)
<i>c</i> (Å)	13.733(8)
β (deg)	103.41(7)
<i>V</i> (Å ³)	4201(6)
<i>Z</i>	4
<i>D</i> _{calc} (g cm ^{–3})	1.747
radiation (λ (Å))	Mo Kα (0.710 69)
μ (cm ^{–1})	11.71
scan type	ω
2θ _{max} (deg)	48.2
no. of refls collected ^a	6670 (+ <i>h</i> , + <i>k</i> , ± <i>l</i>)
no. of unique refls with <i>I</i> > 3σ(<i>I</i>)	3320
no. of variables	567
residuals: ^b <i>R</i> , <i>R</i> _w	0.052, 0.063

^a The intensity data were processed as described in: *CAD 4 and SDP-PLUS User's Manual*; B. A. Frenz & Assoc.: College Station, TX, 1982. The net intensity *I* = [*K*(*NPI*)](*C* – 2*B*), where *K* = 20.1166 (attenuator factor), *NPI* = ratio of fastest possible scan rate to scan rate for the measurement, *C* = total count, and *B* = total background count. The standard deviation in the net intensity is given by [σ(*I*)]² = (*k*/*NPI*)²[*C* + 4*B* + (*pI*)²] where *p* is a factor used to downweight intense reflections. The observed structure factor amplitude *F*_o is given by *F*_o = (*I*/*Lp*)^{1/2}, where *Lp* = Lorentz–polarization factor. The σ(*I*)'s were converted to the estimated errors in the relative structure factors σ(*F*_o) by σ(*F*_o) = 1/2[σ(*I*)/*I*]*F*_o. ^b *R* = Σ|*F*_o – |*F*_c||Σ|*F*_o|; *R*_w = [(Σw(|*F*_o – |*F*_c||)²/Σw*F*_o²)]^{1/2}.

of fractional atomic coordinates, thermal factors, and bond lengths and angles are provided in the supplementary material.

Physical Methods. Visible spectra were recorded on a Hewlett-Packard 8541A diode array spectrometer, while near-infrared absorption data were obtained on a Cary 14 instrument. Raman spectra were obtained on a Spex 1403 spectrometer interfaced with a Spex DM3000 data acquisition system. A Spectra-Physics 2030 argon ion laser was used to pump a 375B tunable dye laser using Rhodamine 6G dye (Exciton, Inc.). Solid samples were pressed into a KBr pellet containing Na₂SO₄ and spun during laser excitation. Raman frequencies and intensities were referenced against the 992-cm^{–1} A₁ stretch of the Na₂SO₄ internal standard. ¹H NMR spectra were recorded on an IBM AC 300 spectrometer at 300 MHz. Chemical shifts (in ppm) were referenced to residual protic solvent peaks. Elemental analyses were performed at MHW Laboratories (Phoenix, AZ).

Electrochemical studies were performed with a BAS 100 electrochemical analyzer (Bioanalytical Systems, Inc., West Lafayette, IN). All experiments were performed under nitrogen at ambient temperature in acetonitrile with 0.1 M tetrabutylammonium tetrafluoroborate as the supporting electrolyte. Cyclic voltammograms (CVs) were obtained by using a three-component system consisting of a platinum disk working electrode, a platinum wire auxiliary electrode, and a BAS saturated calomel reference electrode containing a vycor plug to separate it from the bulk solution. The potentials were referenced to the ferrocenium/ferrocene couple (+395 mV vs SCE).

Magnetic susceptibility data were recorded over a temperature range of 10–300 K at a measuring field of 2.0 kOe with an SHE Corp. VTS-50 superconducting SQUID susceptometer interfaced to an IBM 9000 computer system. Calibration and operating procedures have been reported elsewhere.¹⁶

EPR spectra were obtained at the X-band frequency with a Varian E-109 spectrometer equipped with an Oxford Instruments ESR-10 liquid-helium cryostat. The power saturation experiments were carried out and analyzed by following the protocol of Pearce et al.¹⁷ The temperature-dependence study was carried out with a calibrated carbon glass resistor (CGR-1-1000, Lakeshore Cryotronics) immersed in the sample and sealed with wax. The EPR tube was positioned vertically to minimize impurity signals from the resistor. The leads of the resistor were replaced with a phosphor bronze wire to minimize heat input.

- (10) Norman, R. E.; Holz, R. C.; Zhang, J. H.; O'Connor, C. J.; Menage, S.; Que, L., Jr. *Inorg. Chem.* **1990**, *29*, 4629–4637.
 (11) (a) Anderegg, G.; Wenk, F. *Helv. Chim. Acta* **1967**, *50*, 2330–2332. (b) Gafford, B. G.; Holwerda, R. A. *Inorg. Chem.* **1989**, *28*, 60–66.
 (12) Walker, N.; Stuart, D. *Acta Crystallogr.* **1983**, *A39*, 158–166.
 (13) Gilmore, C. J. *J. Appl. Cryst.* **1984**, *17*, 42–46.
 (14) Cromer, D. T.; Waber, J. T. *International Tables for X-ray Crystallography*; Kynoch Press: Birmingham, England, 1974; Vol. IV, Table 2.2 A.
 (15) Cromer, D. T. *International Tables for X-ray Crystallography*; Kynoch Press: Birmingham, England, 1974; Vol. IV, Table 2.3.1.

- (16) O'Connor, C. J. *Prog. Inorg. Chem.* **1979**, *29*, 204–283.
 (17) Pearce, L. L.; Kurtz, D. M., Jr.; Xia, Y.-M.; Debrunner, P. G. *J. Am. Chem. Soc.* **1987**, *109*, 7286–7293.

Table II. Atomic Coordinates and B_{eq} Values for the Non-Hydrogen Atoms of **9**, $[\text{Fe}_2\text{O}(\text{TPA})_2(\text{MoO}_4)](\text{ClO}_4)_2$

atom	x	y	z	B_{eq}^a (\AA^2)
Fe1	1.1920(1)	0.34632(6)	0.6803(1)	1.29(6)
Fe(2)	1.2715(1)	0.23780(6)	0.5602(1)	1.34(6)
O12	1.2747(6)	0.2929(3)	0.6452(5)	1.4(3)
Mo1	1.01041(8)	0.27094(4)	0.52088(7)	1.60(4)
O2	1.1221(6)	0.2464(3)	0.4771(5)	1.6(3)
O3	1.0562(6)	0.3327(3)	0.5894(5)	2.0(3)
O4	0.9763(6)	0.2244(3)	0.5997(5)	2.4(3)
O5	0.9045(6)	0.2822(3)	0.4222(5)	2.1(3)
N1A	1.3169(7)	0.3905(3)	0.7905(6)	1.2(3)
N2A	1.2517(8)	0.4073(4)	0.5973(6)	1.8(4)
N3A	1.0992(7)	0.4083(3)	0.7451(6)	1.4(3)
N4A	1.1844(7)	0.3081(3)	0.8192(6)	1.4(3)
C1A	1.349(1)	0.4266(4)	0.6376(8)	1.8(4)
C2A	1.401(1)	0.4634(5)	0.5874(9)	2.8(2)
C3A	1.347(1)	0.4806(5)	0.495(1)	3.2(6)
C4A	1.244(1)	0.4612(5)	0.4516(9)	2.7(5)
C5A	1.199(1)	0.4238(5)	0.5054(8)	2.3(5)
C6A	1.1546(8)	0.4399(4)	0.8165(7)	1.5(4)
C7A	1.106(1)	0.4716(5)	0.8755(8)	2.1(5)
C8A	0.997(1)	0.4717(5)	0.8594(9)	2.8(5)
C9A	0.936(1)	0.4399(4)	0.7843(8)	1.9(5)
C10A	0.990(1)	0.4086(5)	0.7305(8)	2.1(5)
C11A	1.2583(9)	0.3237(4)	0.8986(7)	1.6(4)
C12A	1.252(1)	0.3107(4)	0.9964(8)	1.9(5)
C13A	1.167(1)	0.2780(5)	1.0068(8)	2.2(5)
C14A	1.093(1)	0.2605(5)	0.9238(8)	2.0(5)
C15A	1.1026(9)	0.2770(4)	0.8313(8)	1.8(5)
C16A	1.404(1)	0.4027(5)	0.7375(8)	2.1(5)
C17A	1.275(1)	0.4415(4)	0.8253(8)	1.9(5)
C18A	1.354(1)	0.3533(4)	0.8756(8)	1.9(5)
N1B	1.2743(8)	0.1685(4)	0.4545(6)	1.8(4)
N2B	1.2163(7)	0.1707(3)	0.6317(6)	1.6(4)
N3B	1.4259(7)	0.2013(3)	0.6244(6)	1.5(4)
N4B	1.3273(7)	0.2733(4)	0.4410(6)	1.6(4)
C1B	1.177(1)	0.1290(4)	0.5716(8)	1.8(4)
C2B	1.127(1)	0.0854(5)	0.6080(8)	2.2(5)
C3B	1.114(1)	0.0865(5)	0.7047(9)	2.6(5)
C4B	1.154(1)	0.1299(5)	0.7651(8)	2.3(5)
C5B	1.2075(9)	0.1708(4)	0.7276(8)	2.0(4)
C6B	1.4513(9)	0.1557(4)	0.5804(7)	1.8(4)
C7B	1.538(1)	0.1250(5)	0.6223(8)	2.5(5)
C8B	1.600(1)	0.1390(5)	0.7141(9)	2.6(5)
C9B	1.574(1)	0.1846(4)	0.7610(8)	2.0(5)
C10B	1.4879(9)	0.2146(4)	0.7129(8)	1.8(4)
C11B	1.3102(8)	0.2461(4)	0.3636(7)	1.5(4)
C12B	1.338(1)	0.2674(5)	0.2705(8)	1.9(4)
C13B	1.378(1)	0.3194(5)	0.2744(8)	2.1(5)
C14B	1.3931(9)	0.3481(4)	0.3624(7)	1.8(4)
C15B	1.3698(9)	0.3240(4)	0.4455(8)	1.4(4)
C16B	1.189(1)	0.1320(5)	0.4656(8)	2.2(5)
C17B	1.383(1)	0.1415(4)	0.4777(8)	2.0(5)
C18B	1.255(1)	0.1919(4)	0.3524(8)	1.7(4)
Cl1X	0.1510(2)	0.1338(1)	0.1076(2)	2.1(1)
O1X	0.2570(7)	0.1560(3)	0.1168(6)	2.7(4)
O2X	0.1557(7)	0.0902(4)	0.1781(6)	3.4(4)
O3X	0.1092(7)	0.1138(3)	0.0077(6)	3.3(4)
O4X	0.0809(7)	0.1754(3)	0.1302(6)	2.8(4)
Cl1Y	0.8382(2)	0.0250(1)	0.6394(2)	2.1(1)
O1Y	0.8683(9)	0.0346(4)	0.7436(7)	5.0(5)
O2Y	0.9225(9)	-0.0056(4)	0.6122(7)	4.4(5)
O3Y	0.7405(8)	-0.0065(4)	0.6126(7)	4.0(5)
O4Y	0.8271(8)	0.0749(4)	0.5878(7)	4.9(5)
N1Z	0.356(1)	0.0808(6)	0.962(1)	6.6(4)
C1Z	0.400(2)	0.0567(9)	0.890(2)	7.1(5)
C2Z	0.443(3)	0.036(1)	0.836(2)	12(1)

$$^a B_{\text{eq}} = (8/3)\pi^2 \sum_i \sum_j U_{ij} a_i^* a_j^* a_i a_j$$

Results and Discussion

Many of the structural and spectroscopic properties of (μ -oxo)diiron(III) centers are now well understood, particularly with carboxylate ligands bridging the dinuclear center. However, there has yet to be reported a systematic investigation of the effects of bridging tetraoxo anions on the structural and spectroscopic

Table III. Relevant Distances and Angles for $[\text{Fe}_2\text{O}(\text{TPA})_2(\text{L})](\text{ClO}_4)_n$ Complexes^a

parameter ^a	1 (L = carbonate)	2 (L = acetate)	6 (L = diphenyl phosphate)	9 (L = molybdate)	10 (L = phthalate)
Fe1...Fe2	3.196(2)	3.243(1)	3.357(3)	3.421(3)	3.402(2)
Fe1-O12- Fe2	125.4(3)	129.2(2)	138.1(2)	142.9(4)	143.4(3)
Fe1-O12	1.817(5)	1.799(4)	1.815(3)	1.822(7)	1.799(5)
Fe2-O12	1.784(5)	1.790(3)	1.779(3)	1.787(7)	1.785(5)
Fe1-O3	1.911(6)	1.974(3)	1.963(3)	1.913(8)	1.924(5)
Fe2-O2	1.953(6)	2.036(4)	2.045(3)	1.990(7)	1.956(5)
Fe1-N1A	2.204(7)	2.198(3)	2.178(4)	2.212(8)	2.200(6)
Fe1-N2A	2.137(7)	2.126(4)	2.122(4)	2.130(1)	2.133(7)
Fe1-N3A	2.205(6)	2.124(6)	2.184(4)	2.239(9)	2.209(6)
Fe1-N4A	2.112(7)	2.200(6)	2.120(4)	2.149(8)	2.139(7)
Fe2-N1B	2.245(7)	2.237(4)	2.239(4)	2.250(9)	2.228(7)
Fe2-N2B	2.149(8)	2.133(4)	2.127(4)	2.127(9)	2.192(6)
Fe2-N3B	2.156(8)	2.157(4)	2.130(4)	2.160(1)	2.242(6)
Fe2-N4B	2.158(9)	2.105(4)	2.121(4)	2.119(9)	2.164(8)

^a All distances are in angstroms, and all angles are in degrees. For labels, see ORTEP drawings. O2 and O3 are the O₂X labels.

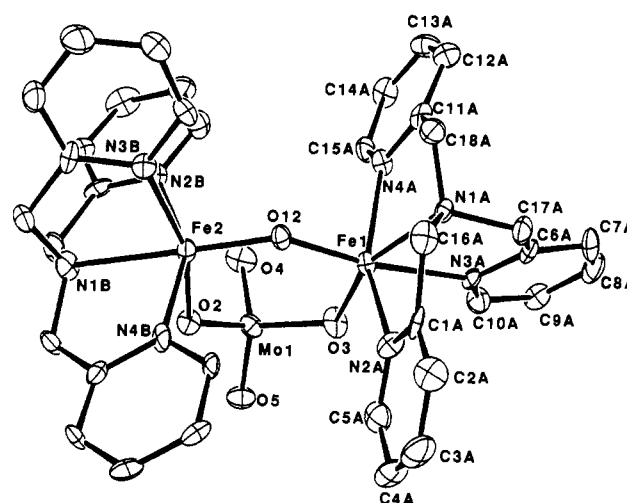


Figure 1. ORTEP (ORNL-5138, Oak Ridge National Laboratory, 1976) plot for **9**, $[\text{Fe}_2\text{O}(\text{TPA})_2(\text{MoO}_4)]^{2+}$, showing a partial numbering scheme. The carbon atoms on the TPA bound to Fe2 are numbered analogously to those on the TPA bound to Fe1.

properties of this structural motif. We have synthesized a new series of $[\text{Fe}_2\text{O}(\text{TPA})_2(\text{L})](\text{ClO}_4)_2$ complexes, where L is sulfate (**4**), phosphate (**5**), arsenate (**7**), vanadate (**8**), and molybdate (**9**). This series of tetraoxo anion complexes represents the first extensive series having the same binding stoichiometry as the PAP-anion complexes with which to compare their physical and spectral properties. To augment this series, several previously reported and crystallographically characterized (μ -oxo)diiron(III) complexes are included,^{6b,10} where L is carbonate (**1**), acetate (**2**), benzoate (**3**), diphenyl phosphate (**6**), and phthalate (**10**). This enlarged series of (μ -oxo)diiron(III) complexes has enabled us to explore the effects of the Fe-O-Fe angle on the spectral and Raman properties of the (μ -oxo)diiron(III) core, their electrochemical properties, and the EPR properties of the corresponding mixed-valence complexes.

Structural Studies. X-ray diffraction studies were conducted on $[\text{Fe}_2\text{O}(\text{TPA})_2(\text{MoO}_4)](\text{ClO}_4)_2 \cdot \text{CH}_3\text{CN}$ (**9**), the only (μ -oxo)diiron(III) complex with a bridging molybdate to be structurally characterized. The cation of **9** is shown in Figure 1, while relevant bond distances and angles are collected in Table III along with pertinent parameters of previously reported $[\text{Fe}_2\text{O}(\text{TPA})_2(\text{L})](\text{ClO}_4)_{2 \text{ or } 3}$ complexes for comparison. The structure confirms

Table IV. Electronic and Magnetic Properties of [Fe₂O(TPA)₂(L)](ClO₄)₃ Tetraoxo Anion Complexes

parameter	1 (L = CO ₃)	4 (L = SO ₄)	5 (L = HPO ₄)	7 (L = HAsO ₄)	8 (L = HVO ₄)	9 (L = MoO ₄)	
Electronic Properties							
λ _{max} (nm) (ε (mM ⁻¹ cm ⁻¹))	335 (10) 372 (7.6) 425 (sh) 450 (1.1) 500 (1.0) 535 (sh) 700 (0.15) 980 (0.005)	316 (9) 366 (5.8) 420 (sh) 450 (sh) 490 (0.63) 520 (0.19) 658 (0.13) 1030 (0.014)	318 (9) 360 (6.2) 420 (sh) 440 (sh) 484 (0.49) 514 (0.19) 638 (0.14) 980 (0.012)	324 (9) 360 (6.5) 415 (sh) 446 (sh) 486 (0.57) 515 (0.20) 630 (0.15) 980 (0.013)	314 (9) 372 (3.6) 420 (sh) 445 (sh) 491 (0.41)	314 (8) 374 (4.3) 410 (sh) 427 (sh) 499 (0.45)	314 (8) 374 (4.3) 410 (sh) 427 (sh) 499 (0.45)
Magnetic Properties							
-J (cm ⁻¹)	108.4	106.6	102.8	100.2		100.8	
TIP (cgsu/mol)	0.000 215	0.000 18	0.001 25	0.0002		0.000 52	
p (mol %)	0.16	0.18	0.79	0.01		0.47	
g	2.02	2.00	2.06	2.05		2.05	

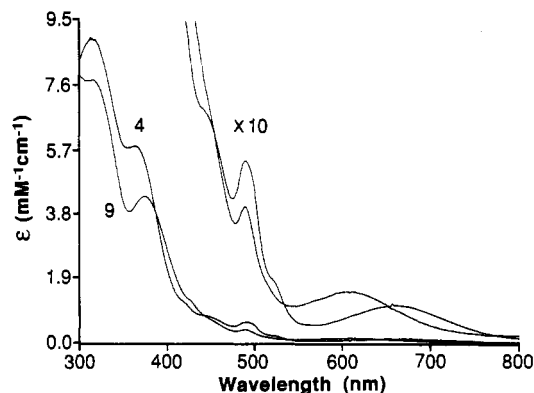
the presence of a (μ-oxo)diferric core with a single bridging molybdate, which is the correct stoichiometry of PAP-molybdate interactions.

The structure of **9** resembles those of previously reported [Fe₂O(TPA)₂(L)](ClO₄)₂ or ₃ complexes in that the (μ-oxo)diiron(III) core contains distinct iron sites with a distorted octahedral geometry (Figure 1). In complexes of this type, the tertiary amine on Fe1 is cis to the oxo bridge while the tertiary amine on Fe2 is trans to the oxo bridge. Consequently, this arrangement avoids potential steric interactions between the pyridine C3-H protons of the two TPA ligands, which would exist in a symmetric complex where both tertiary amines would be trans to the oxo bridge. This ligand configuration produces differences between Fe1- and Fe2-O_{oxo}, -N_{amine}, and -N_{pyridine} bond lengths which are typical of complexes in this series (Table III).

Complex **9** has the largest Fe...Fe separation (3.421 Å) among our entire series of dibridged TPA complexes, consistent with the large "bite" angle of the molybdate dianion. The higher charge of molybdate compared to carboxylate ligands is also reflected in the core dimensions of the (μ-oxo)diiron(III) unit. Although the average Fe-O_{oxo} and Fe-N_{TPA} bond lengths for **9** are comparable to those of the monoanion bridged complexes, the average Fe-O_{molybdate} bond length is shorter (1.95 Å) compared to the corresponding Fe-O bond lengths found for **2**, **3**, and **6** (2.01 Å) yet nearly equal to that of the dianion carbonate (1.94 Å). These small changes in core dimension along with the larger "bite" angle of molybdate likely cause the large Fe-O-Fe angle of 142.9°.

Only two complexes of this type have been found to have Fe-O-Fe angles greater than 140°, namely, those with bridging molybdate and phthalate ligands. These two (μ-oxo)diiron(III) TPA complexes contain very similar Fe-O-Fe angles (142.9 vs 143.4° for molybdate and phthalate, respectively), identical average Fe-O_{oxo} bond lengths (1.80 Å), and similar Fe-O_{ligand} average bond lengths (1.95 vs 1.94 Å). However, subtle differences in their respective Fe...Fe separations (3.421 vs 3.402 Å) and average Fe-N_{TPA} bond lengths (2.17 vs 2.21 Å) belie a more significant structural difference. As previously reported,¹⁰ the phthalate-bridged complex contains TPA capping ligands, with the oxo bridge trans to a pyridine on each iron center, thereby providing a pseudo-2-fold axis of symmetry about the Fe-O-Fe core. In contrast, the TPA ligands in **9** adopt the unsymmetric arrangement found in all the TPA complexes with smaller Fe-O-Fe angles. At present, it is not clear what subtle factors determine the structural motif adopted by these complexes.

In solution, **9** maintains the unsymmetrical structural motif, as indicated by the multiplicity of the NMR resonances (see supplementary material).^{6b,10} The NMR spectra of the other tetraoxo anion bridged complexes also indicate that the TPA capping ligands adopt the unsymmetric arrangement in these complexes.

Figure 2. UV-visible spectra of **4** and **9** in CH₃CN.

Magnetic properties. The magnetic properties of the new TPA complexes are similar to those of other complexes in the series (Table IV). The *J* values for the tetraoxo anion complexes all hover near -100 cm⁻¹ ($H = -2JS_1 \cdot S_2$). As noted previously, there is no obvious dependence of the antiferromagnetic interaction on Fe-μ-O-Fe angle.¹⁰

Electronic and Vibrational Properties. The absorption data for the tetraoxo anion complexes are found in Table IV, and the visible absorption spectra of **4** and **9** are shown in Figure 2. The electronic spectrum of each (μ-oxo)diiron(III) complex consists of intense features in the near-UV, weaker bands in the 400–550-nm region, and still weaker features in the 550–1000-nm region. These spectra are very similar to those found for all of the previously reported members of this series^{6b,10} (Table IV), reflecting the similarities in the structures of these complexes.

The electronic spectra of (μ-oxo)diiron(III) complexes have been shown to be quite sensitive to structural variations about the diiron core.^{5–7,10} In particular, changes in ligand basicity, charge, and bite angle result in significant perturbations of the observed electronic transitions. It is clear from these and previously reported data on (μ-oxo)diiron(III) complexes that as the Fe-O-Fe angle increases, the 400–500-nm absorption bands blue-shift (except the band near 490 nm) and the extinction coefficients decrease. Solomon *et al.*¹⁸ suggested that these bands are principally weak oxo-to-iron(III) ligand-to-metal charge transfer (LMCT) transitions, so that the observed blue shift arises from the increased π bonding between the iron atoms and the μ-oxo atom as the Fe-O-Fe angle approaches 180°. The charge-transfer assignment is corroborated by the resonance Raman studies of Sanders-Loehr *et al.*,¹⁹ as excitation between 350 and 600 nm results in significant resonance enhancement of the Raman-active symmetric Fe-O-Fe vibrational mode, ν_s(Fe-O-Fe). The rel-

(18) Reem, R. C.; McCormick, J. M.; Richardson, D. E.; Devlin, F. J.; Stephens, P. J.; Musselman, R. L.; Solomon, E. I. *J. Am. Chem. Soc.* 1989, 111, 4688–4704.

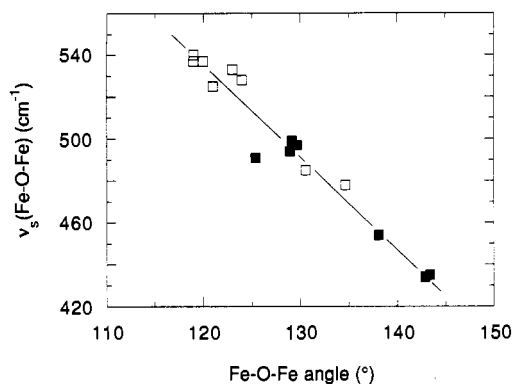


Figure 3. Correlation between the $\nu_s(\text{Fe-O-Fe})$ features and the Fe-O-Fe angles of $(\mu\text{-oxo})\text{diiron(III)}$ complexes supported by carboxylate or oxoanion bridges. Filled squares represent data for structurally characterized $[\text{Fe}_2\text{O}(\text{TPA})_2]$ complexes, while open squares represent data for structurally characterized tribringed $(\mu\text{-oxo})\text{diiron(III)}$ complexes from refs 7b and 19.

actively invariant band near 490 nm was assigned to the ${}^6\text{A}_1 \rightarrow ({}^4\text{E}, {}^4\text{A})$ ligand field transition, which is insensitive to ligand field strength.

The near-IR bands of this series are found at 950–1050 nm (ϵ ca. $0.010 \text{ mM}^{-1}\text{cm}^{-1}$) (Table IV); they are insensitive to the Fe-O-Fe angle but instead shift relative to the net charge and basicity of the bridging anionic ligand. They were previously assigned by Solomon *et al.* as the lowest energy ${}^6\text{A}_1 \rightarrow {}^4\text{T}_1$ ligand field transition of the ferric ions on the basis of circular dichroism and absorption studies of metHr and its anion complexes;¹⁸ this assignment is consistent with the observed trends in our present data and with those previously reported for the $(\mu\text{-oxo})\text{diiron(III)}$ TPA series.^{6b,10}

There is some disagreement in the assignment of the features in the region 550–700 nm ($\epsilon \sim 0.15 \text{ mM}^{-1}\text{cm}^{-1}$) (Table IV). Unlike the near-IR band, this feature is quite sensitive to the Fe-O-Fe angle, blue-shifting from 705 to 550 nm as the angle changes from 125 to 180° , irrespective of ligand field strength (Table IV). This blue shift is similar to that observed for the bands in the 400–500-nm region, which have been assigned to oxo-to- Fe(III) LMCT transitions. From their study of metHrX complexes, Solomon *et al.* noted that the metHr feature in this region had a dependence on the ligand field strength of X and assigned this band to the ${}^6\text{A}_1 \rightarrow {}^4\text{T}_2$ ligand field transition.¹⁸ However the position of this band in such an assignment would be insensitive to the Fe-O-Fe angle, just like the near-IR feature. Since this band shows a marked dependence on the Fe-O-Fe angle in our series of $(\mu\text{-oxo})\text{diiron(III)}$ complexes, we conclude that the features we observe in the 550–700-nm region have dominant oxo-Fe LMCT character.

The Raman spectra of this series of complexes show the enhancement of a feature at 400–500 cm^{-1} associated with the $\nu_s(\text{Fe-O-Fe})$ mode. Interestingly, when the Raman spectra of $[\text{Fe}_2\text{O}(\text{TPA})_2(\text{acetate})](\text{ClO}_4)_3$ (**2**) and $[\text{Fe}_2\text{O}(\text{TPA})_2(\text{phthalate})](\text{ClO}_4)_2$ (**10**) with 640-nm excitation are compared, the ν_s mode is 2-fold more enhanced in the case of **10** than in the case of **2**. Since **10** and **2** exhibit bands at 604 and 705 nm, respectively, the stronger enhancement for **10** further supports the notion that the absorption feature in the 600–700-nm region has significant charge-transfer character.

Our Raman data provide further useful information. Sanders-Loehr *et al.*¹⁹ have established a nearly linear dependence between the frequency of the $\nu_s(\text{Fe-O-Fe})$ mode and the Fe-O-Fe angle in oxo-bridged dinuclear iron centers of non-heme proteins and model compounds. The ν_s frequencies and Fe-O-Fe angles for our crystallographically characterized $[\text{Fe}_2\text{O}(\text{TPA})_2(\text{L})](\text{ClO}_4)_{2 \text{ or } 3}$

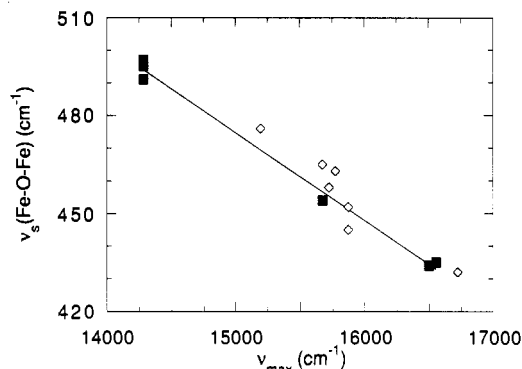


Figure 4. Correlation between the $\nu_s(\text{Fe-O-Fe})$ and the absorption features of dibridged $(\mu\text{-oxo})\text{diiron(III)}$ TPA complexes. Filled squares represent data for structurally characterized complexes, while diamonds represent data for related complexes which do not have crystal structures.

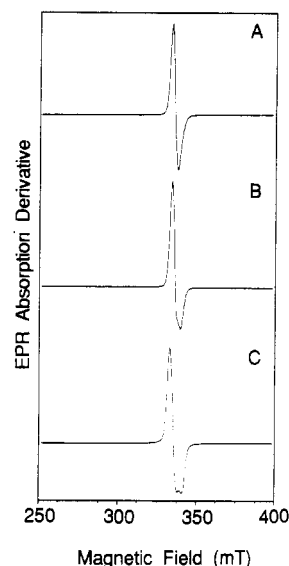


Figure 5. EPR spectra of mixed-valence diiron complexes obtained by cobaltocene treatment of (A) $[\text{Fe}_2\text{O}(\text{TPA})_2\{\text{O}_2\text{P}(\text{OPh})_2\}_2]^{3+}$, (B) $[\text{Fe}_2\text{O}(\text{TPA})_2\text{MoO}_4]^{2+}$, and (C) $[\text{Fe}_2\text{O}(\text{TPA})_2\text{Cl}_2]^{2+}$ in CH_3CN at 4 K.

complexes demonstrate a similar linear correlation (Figure 3; Table V). Furthermore the energy of the 550–700-nm band also correlates linearly with the Fe-O-Fe angle, thus supporting the oxo-to-iron LMCT assignment for these bands (not shown). As shown in Figure 4, there is thus a linear correlation between ν_s and the energy of the 550–700-nm absorption band for all complexes in the TPA series. This strong correlation allows us to empirically estimate the Fe-O-Fe angle for compounds which have not been crystallographically characterized, on the basis of UV-vis and Raman data. Indeed, the estimated Fe-O-Fe angles (Table V) for the complexes which are not crystallographically characterized are consistent with expectations based on the bite distances of these bridges.

EPR Spectroscopy. A number of the $[\text{Fe}_2\text{O}(\text{TPA})_2(\text{L})](\text{ClO}_4)_{2 \text{ or } 3}$ complexes in this study are readily reduced by cobaltocene to afford mixed-valent species with EPR properties of relevance to the diiron-oxo proteins. The mixed-valent complexes (where L = acetate, sulfate, phosphate, arsenate, diphenyl phosphate, molybdate, or dichloride) generated at room temperature and rapidly cooled to 77 K exhibit EPR signals with g values less than 2.0 (Figure 5). These signals are typical of antiferromagnetically coupled dinuclear centers consisting of a high-spin (${}^6\text{A}$) Fe(III) ion and a high-spin (${}^3\text{T}$) Fe(II) ion resulting in an $S = 1/2$ ground state.^{2b} Integration of these signals relative to a copper(II) sulfate standard indicates that $\sim 60\%$ of the starting species is in the mixed-valent oxidation state in each case.

(19) Sanders-Loehr, J.; Wheeler, W. D.; Shiemke, A. K.; Averill, B. A.; Loehr, T. M. *J. Am. Chem. Soc.* **1989**, *111*, 8084–8093.

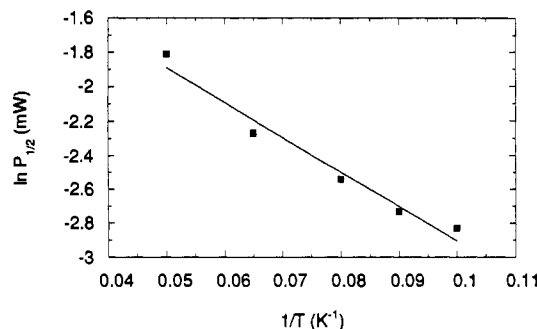


Figure 6. Temperature dependence of the power saturation behavior of the mixed-valence EPR spectrum derived from the cobaltocene reduction of $[\text{Fe}_2\text{O}(\text{TPA})_2(\text{O}_2\text{P}(\text{OPh})_2)_2]^{3+}$.

Isotropic EPR signals with $g = 1.95$ are observed for the acetate, sulfate, phosphate, and arsenate complexes, while axial signals are exhibited by the diphenyl phosphate ($g_{\perp} = 1.95$; $g_{\parallel} = 1.92$), molybdate ($g_{\perp} = 1.95$; $g_{\parallel} = 1.92$), and dichloride ($g_{\perp} = 1.96$; $g_{\parallel} = 1.92$) derivatives. Similarly, the mixed-valent derivative of $[\text{Fe}_2\text{O}(\text{Me}_3\text{TACN})_2(\text{OAc})_2](\text{PF}_6)_2$ generated by chemical or electrochemical reduction exhibits a signal with $g_{\perp} = 1.95$ and $g_{\parallel} = 1.89$.^{5b} At present, it is not clear what factors determine the anisotropy of the mixed-valent species, but the model complexes all show much smaller anisotropies than found for semimetHrs,^{17,18} mixed-valent MMO,²⁰ or the reduced PAPS.^{2b}

The temperature dependence of the power saturation of the mixed-valent signals can provide an estimate of the strength of antiferromagnetic coupling between the two metal centers.¹⁷ For the mixed-valent derivative of **6**, the first excited state was estimated to be 28.5 cm^{-1} above the $S' = 1/2$ ground state corresponding to a $2J$ value of $-19 (\pm 1) \text{ cm}^{-1}$ ($H = -2J S_1 S_2$) (Figure 6), a value substantially weaker than that of the (μ-oxo)diferroc starting material ($2J = -208 \text{ cm}^{-1}$). Similar $2J$ values of $-18 (\pm 1)$ and $-19 (\pm 1) \text{ cm}^{-1}$ are found for the corresponding acetate and benzoate complexes, respectively. The values found for the mixed-valent TPA complexes are comparable to those of semimetHrN₃ and semimetHr_R determined from EPR ($2J = -30 \text{ cm}^{-1}$)¹⁷ and MCD measurements ($2J = -16 \text{ cm}^{-1}$)²¹ and that determined for reduced uteroferrin ($2J = -20 \text{ cm}^{-1}$) from magnetic susceptibility measurements.²²

Electrochemistry. A systematic study of the reduction potentials (E_m) of complexes which model the (μ-oxo)diiron(III) core has yet to be reported. The broad range in bridging ligand basicity and the variation in charge for our series of (μ-oxo)diiron(III) TPA complexes prompted us to explore their redox properties for comparison with those of the diiron-oxo proteins. The results of the cyclic voltammetry experiments are found in Table VI. The CV of **9** (shown in Figure 7) consists of a single reversible wave centered at -170 mV vs NHE. Nearly all of the (μ-oxo)diiron(III) complexes in this series exhibit reversible one-electron reductions. For comparison, the $\text{Fe}^{\text{III}}\text{Fe}^{\text{III}}/\text{Fe}^{\text{III}}\text{Fe}^{\text{II}}$ reduction potentials of some previously reported (μ-oxo)diiron(III) complexes are included in Table VI.⁵

Inspection of Table VI indicates that in general the E_m values of (μ-oxo)diiron(III) TPA complexes depend on the basicity and charge of the bridging anionic ligands. The monoanionic complexes (**2**, **3**, **6**, and **B**) fall into a group which have E_m values that range from $+180$ to $+65 \text{ mV}$ vs NHE, while the dianionic complexes (**1**, **4**, **5**, **7–10**, **C**, and **E**) have E_m values which range from -35 to -380 mV vs NHE. The diphenyl phosphate complex (**6**) has the most positive E_m value ($+180 \text{ mV}$), corresponding to the least basic of the monoanions. As the basicity of the bridge

Table V. Spectroscopic Properties of $[\text{Fe}_2\text{O}(\text{TPA})_2(\text{L})](\text{ClO}_4)_2$ or 3 Complexes

anion	E (cm^{-1})	$\nu_1(\text{FeOFe})$ (cm^{-1})	$\angle\text{FeOFe}$ (deg) ^a	Fe-O_{av} (Å)
CO ₃	14 286	491	125.4	1.801(5)
OAc	14 286	495	129.2	1.795(4)
OBz	14 286	497	129.7	1.791(3)
SO ₄	15 198	476	(134)	
HPO ₄	15 674	465	(138)	
O ₂ P(OPh) ₂	15 674	454	138.1	1.797(5)
O ₂ P(Ph) ₂	15 723	458	(138)	
O ₃ P(OPh)	15 773	463	(138)	
HAsO ₄	15 873	452	(139)	
HVO ₄	15 873	445	(139)	
MoO ₄	16 502	434	142.9	1.805(7)
phthalate	16 556	435	143.4	1.792(5)
maleate	16 722	432	(145)	

^a Values in parentheses represent estimates based on the correlation in Figure 4 using the equation $y = 31.7 + (6.76 \times 10^{-3})x$.

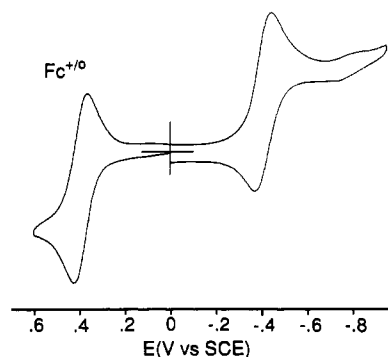


Figure 7. Cyclic voltammogram of $[\text{Fe}_2\text{O}(\text{TPA})_2\text{MoO}_4](\text{ClO}_4)_2$ in CH_3CN with 0.1 M tetrabutylammonium tetrafluoroborate as supporting electrolyte, referenced to the ferrocenium/ferrocene couple.

increases, the E_m values for these complexes become more negative, which is consistent with the addition of more negative charge to the diiron core. Thus the very basic carbonate (**1**) has the most negative potential. However, the E_m values for the complexes in the series do not strictly correlate with the ligand basicity. Since the basicity of the oxo bridge decreases as the Fe–O–Fe angle increases, the effect of increased charge may be mitigated by an increase of the Fe–O–Fe angle. Thus the E_m values of this extensive series reflect both ligand basicity and Fe–O–Fe angle.

Consideration of the E_m values of other (μ-oxo)diferroc complexes⁵ indicates that the general trends observed for our TPA series, i.e. decreasing E_m values with increasing ligand charge and basicity and increasing E_m values with increasing angle, apply regardless of capping ligand. Complex **A** (Table VI), with its FeN_3O site, is the most positive at $+348 \text{ mV}$ vs NHE,^{5c} while **C**, with its FeN_4OCl site, is considerably more negative (-45 mV vs NHE). The difference in reduction potential of these two crystallographically characterized complexes with unsupported μ-oxo bridges is presumably due to the added charge of the chloride ion in **C**. Comparison of the E_m values of complexes with one or more bridging carboxylate ligands provides a similar trend. The two (μ-oxo)(μ-carboxylato)diiron(III) TPA complexes **2** and **3** ($+170$ and $+150 \text{ mV}$ vs NHE, respectively) (Table VI) possess FeN_4O_2 sites and have E_m values that are more positive than those of the (μ-oxo)bis(μ-carboxylato) complexes **D** and **F** (-130 ^{5b} and -470 ^{5a} mV vs NHE) (Table VI), which possess FeN_3O_3 sites. Though **D** and **F** both have FeN_3O_3 sites, **F** exhibits a substantially more negative potential due to the negatively charged HB(pz)₃ ligand.

Structural Implications for Diiron–Oxo Proteins. Among diiron proteins, metHr and R2 have been crystallographically characterized to have (μ-oxo)diferroc centers.^{3,4} MetHr with its (μ-oxo)bis(μ-carboxylato)diiron(III) unit and five terminal histidine ligands has an $\text{Fe}^{\text{III}}\text{Fe}^{\text{III}}/\text{Fe}^{\text{III}}\text{Fe}^{\text{II}}$ potential of $+110 \text{ mV}$ vs

(20) Fox, B. G.; Surer, K. K.; Münck, E.; Lipscomb, J. D. *J. Biol. Chem.* **1988**, *263*, 10553–10556.

(21) McCormick, J. M.; Reem, R. C.; Solomon, E. I. *J. Am. Chem. Soc.* **1991**, *113*, 9066–9079.

(22) Day, E. P.; David, S. S.; Peterson, J.; Dunham, W. R.; Bonvoisin, J. J.; Sands, R. H.; Que, L., Jr. *J. Biol. Chem.* **1988**, *263*, 15561–15567.

Table VI. Fe(III)/Fe(II) Reduction Potentials (mV vs NHE) for High-Spin Fe(III)/Fe(II) Couples of (μ -oxo)diiron(III) TPA and Relevant Model Complexes

complex	anion or cation ^a	$E_{1/2}$	ΔE	reversibility
A	[N5FeOFeCl ₃]	+348		
6	O ₂ P(OPh) ₂	+180	70	R
3	OBz	+170	70	R
2	OAc	+150	70	R
B	O ₂ P(Ph) ₂	+65	65	R
8	HVO ₄	-35	70	R
C	2 Cl	-45	80	R
4	SO ₄	-115	70	R
7	HAsO ₄	-120	65	R
D	[Fe ₂ O(Me ₃ TACN) ₂ (OAc) ₂] ²⁺	-130		
9	MoO ₄	-170	75	R
5	HPO ₄	-175		IR
10	phthalate	-185	100	QR
E	O ₃ P(OPh)	-310	70	R
1	CO ₃	-380		IR
F	[Fe ₂ O(HB(pz) ₃) ₂ (OAc) ₂]	-470		

^a N5 = *N*-(hydroxyethyl)-*N,N',N'*-tris(2-benzimidazolylmethyl)-1,2-diaminoethane; Me₃TACN = 1,4,7-trimethyl-1,4,7-triazacyclononane; HB(pz)₃ = hydrotris(pyrazolyl)borate.

Table VII. Reduction Potentials (mV vs NHE) for Fe(III)/Fe(II) Couples of Diiron-Oxo Proteins

enzyme	E_m	pH	ref
uteroferrin-MoO ₄	+498	6.0	25
uteroferrin	+306	6.0	25
uteroferrin-AsO ₄	+217	6.0	25
uteroferrin-PO ₄	+113	6.0	25
hemerythrin [met/(semimet) _R]	+110	8.2	23a
myohemerythrin [met/(semimet) _R]	+70	8.2	23a
methane monooxygenase [E ₁]	+48	7.0	23c
ribonucleotide reductase R2	≥-110	7.5	23b

NHE.^{23a} Interestingly, the metHr value is comparable to that of **2**, a complex with a (μ -oxo)(μ -carboxylato) core, but significantly more positive than those found for **D** and **F**, complexes with (μ -oxo)bis(μ -carboxylato) cores that closely match the structure of the hemerythrin diiron core. The positive shift in potential for metHr relative to **D** and **F** suggests that the semimetHr derivative is stabilized relative to the corresponding one-electron-reduced species of **D** and **F**. One mechanism for stabilization that may be available in a protein environment is the protonation of the oxo bridge upon reduction to neutralize the added charge that is introduced. A number of spectroscopic arguments support such a protonation of the oxo bridge, including EXAFS²⁴ and CD data.²¹ Solomon *et al.*²¹ has proposed that the conversion of metHr to semimet_RHr entails the protonation of the oxo bridge and the binding of hydroxide to the five-coordinate iron center upon reduction.

R2, on the other hand, has a (μ -oxo)(μ -carboxylato)diiron(III) core with two terminal histidines and three terminal carboxylate ligands. Its reduction potential has been estimated to be -110 mV vs NHE.^{23b} The more negative potential relative to metHr is explained by the larger number of anionic ligands present in this diiron core. The structure of the mixed-valence form is unclear at present, since this derivative has thus far only fleeting existence and has not been studied in detail.

The redox potentials of uteroferrin (Uf), the purple acid phosphatase from porcine uteri, in the absence and presence of the inhibitors phosphate, arsenate, and molybdate were recently reported.²⁵ For Uf the Fe^{III}Fe^{III}/Fe^{III}Fe^{II} reduction potential was determined to be +306 mV vs NHE at pH 6.01 using coulometric techniques (Table VII). Phosphate and arsenate shift the potential of Uf more *negatively* by 193 and 89 mV, respectively, while molybdate shifts the potential of Uf more *positively* by 192 mV (Table VII). These potential shifts are consistent with the observed susceptibility of reduced Uf to air oxidation. Reduced Uf autoxidizes slowly. The presence of phosphate or arsenate potentiates autoxidation, forming oxidized Uf-phosphate or -arsenate complexes; in contrast, molybdate forms a reduced Uf complex that is air stable.

Comparison of the reduction potentials of Uf with those of our series of (μ -oxo)diiron(III) TPA complexes with bridging tetraoxo anions provides some extremely valuable insight with regard to Uf-tetraoxo anion interactions. While it is unlikely that uteroferrin has the oxo bridge or the nitrogen-rich environment of the TPA series, examination of the trends upon substitution of the bridging anion is instructive. As in the Uf series, the phosphate complex **5** exhibits a more negative reduction potential (by -55 mV) than the corresponding arsenate complex **7**, consistent with the slightly greater basicity of phosphate relative to arsenate. But unlike that in the Uf series, the reduction potential of the molybdate complex **9** is nearly the same as that of the phosphate complex.

Our electrochemical data support the notion that molybdate does not interact in the same way with the Uf diiron site as do phosphate and arsenate. Indeed, the positive shift of the Uf potential observed upon molybdate binding cannot be consistent with the coordination of the anion to the redox-active iron and strongly suggests that it is coordinated only to the redox-inactive Fe(III) center in reduced Uf. Phosphate and arsenate, on the other hand, are proposed to bridge the diiron site as in the model complexes. This proposal is based on the electrochemical data that require phosphate binding at the redox-active Fe center²⁵ and EPR data that show phosphate binding at the redox-inactive Fe(III) center.⁸ This anion-binding scheme supersedes that proposed by David and Que⁸ and is consistent with the EXAFS analysis of uteroferrin-anion complexes.²⁶

Acknowledgment. We thank Professor J. D. Britton for his assistance and expertise with the structure determination and Professor L. L. Miller for the use of the BAS 100 electrochemical analyzer. This work was supported by grants from the National Institutes of Health (GM-38767, L.Q.) and the Louisiana Education Quality Support administered by the Board of Regents of the State of Louisiana and by the donors of the Petroleum Research Fund, administered by the American Chemical Society (C.J.O.). R.C.H. is grateful for an NIH postdoctoral fellowship (GM-13919).

Supplementary Material Available: Tables of NMR parameters, complete bond lengths and angles, and anisotropic thermal parameters for **9** and fits of the susceptibility data (Figures S1-S4) for **4**, **5**, **7**, and **9** (19 pages). Ordering information is given on any current masthead page.

- (23) (a) Armstrong, F. A.; Harrington, P. C.; Wilkins, R. G. *J. Inorg. Biochem.* **1983**, *22*, 83-91. (b) Lam, K.-Y.; Fortier, D. G.; Sykes, A. G. *J. Chem. Soc., Chem. Commun.* **1990**, 1019-1021. (c) Liu, K.; Lippard, S. J. *J. Biol. Chem.* **1991**, *266*, 12836-12839.
- (24) Scarrow, R. C.; Maroney, M. J.; Palmer, S. M.; Que, L., Jr.; Roe, A. L.; Salowe, S. P.; Stubbe, J. *J. Am. Chem. Soc.* **1987**, *109*, 7857-7864.

- (25) Wang, L. D.; Holz, R. C.; David, S. S.; Que, L., Jr.; Stankovich, M. T. *Biochemistry* **1991**, *30*, 8187-8194.

- (26) True, A. E.; Scarrow, R. C.; Randall, C. R.; Holz, R. C.; Que, L., Jr. *J. Am. Chem. Soc.* **1993**, *115*, 4246-4255.